Electronic structure of liquid mercury

1999 J. Phys.: Condens. Matter 11 4597

(http://iopscience.iop.org/0953-8984/11/24/303)

J. Phys.: Condens. Matter **11** (1999) 4597–4615. Printed in the UK PII: S0953-8984(99)00852-8

Electronic structure of liquid mercury

S K Bose

Physics Department, Brock University, St Catharines, Ontario L2S 3A1, Canada

Received 13 January 1999, in final form 8 April 1999

Abstract. The electronic structure of liquid mercury is calculated using the scalar-relativistic tight-binding linear muffin-tin orbitals (TB-LMTO) basis and the recursion method. Calculations are performed for 1372 atom structural models of liquid mercury in the temperature range 150–250 °C, generated via the Metropolis Monte Carlo method and suitable two-body potentials. The existence of a pseudo-gap in the density of states (DOS), as conjectured by Mott, is carefully examined. The calculation produces a lowering of the DOS at the Fermi level with respect to the free electron value. The Mott g-factor is about 70%. The reason for the lowering of the DOS at the Fermi level below the free electron value is the hybridization of the narrow d band with the much broader sp band. This opens the so-called Fano gap in the sp density of states, pushing states from the middle of the sp band to the edges. However, the overall (sp+d) density of states has no deep or pronounced local minimum at the Fermi energy. For comparison, as well as a better understanding of the liquid state electronic structure, the DOS of Hg in various assumed crystalline phases is studied via the scalar-relativistic LMTO-ASA (atomic sphere approximation) method. We also present resistivity results for the temperature range 150–250 °C, calculated by using the Kubo–Greenwood formula and the TB-LMTO-recursion scheme.

1. Introduction

Electronic properties of liquid mercury are remarkably different from most other liquid metals. In particular the dc resistivity is quite large and decreases on addition of most metallic impurities. In order to explain these and other experimental results for liquid mercury Mott [1] advanced the idea of a 'pseudogap', that is, a density of states at the Fermi energy significantly reduced with respect to the free electron value. The existence of the pseudogap was subsequently refuted by Evans [2], who carefully constructed a suitable pseudopotential for mercury, giving particular attention to the d states near the bottom of the conduction band. With the help of this pseudopotential Evans was able to explain most of the resistivity and thermo-electric power data for mercury and its alloys using the Faber–Ziman theory, and without invoking Mott's pseudogap hypothesis. Chan and Ballentine [3] modified Evans' pseudopotential by incorporating an appropriate effective-mass correction to screening. This nonlocal pseudopotential was very similar to one of the pseudopotentials obtained by Jones and Datars [4] by fitting to their Fermi surface measurements for solid mercury. Chan and Ballentine [3] calculated the density of states in liquid mercury using the Green function method and the above nonlocal pseudopotential. Their results show only a small dip of the DOS below the free-electron curve and thus do not corroborate the pseudogap picture. DOS calculations by Itami and Shimoji [5] also show only a small dip. Several other DOS calculations for liquid mercury (see Ballentine [6] for a review) indicate that the pseudogap, if present, lies below rather than at the Fermi energy. The pseudogap conjecture was later withdrawn by Mott [7]

0953-8984/99/244597+19$19.50

as being relevant to the transport properties of mercury at room temperature and pressure, but he still maintained that it may indeed be relevant to explaining the increase in the magnetic susceptibility of mercury with increasing temperature or on addition of indium.

On the experimental front Norris *et al* [8] and Cotti *et al* [9] have reported measurements of the photoemission spectrum of liquid mercury and claim that their data support the pseudogap conjecture for the bulk DOS. The difficulties involved in interpreting the photoemission data are well known as there are both surface and bulk contributions to consider and even the bulk contribution is not directly proportional to the DOS. Both of the above two photoemission studies claim to have taken into account all relevant factors in the interpretation of the data. Recent photoemission work by Oelhafen *et al* [10] also points to the existence of a minimum in the DOS at the Fermi level in liquid mercury, less pronounced than in other heavy liquid polyvalent metals such as Tl, Pb and Bi.

In this paper we present a calculation of the electronic structure of liquid mercury based on density functional theory and realistic structural models for 150 °C and 250 °C. The calculations are performed using the tight-binding linear muffin-tin orbitals (TB-LMTO) basis (Andersen and Jepsen [11]; Andersen *et al* [12]) and the recursion method (Haydock [13]). The electronic structure of solid mercury is also presented for the sake of comparison. Finally, a resistivity calculation for liquid mercury in the temperature range 150–250 °C based on the Kubo–Greenwood formula [14] is presented.

An issue of considerable interest related to electronic structure is the metal–semiconductor transition in expanded liquid Hg, occurring around the density range $\rho \approx 8$–9 g cm^{-3}. This is expected at reduced densities when the 6s and 6p conduction bands no longer overlap. The sharpness of this transition is expected to be diffused as a result of density fluctuations and loss of long- and short-range order in the liquid state. Mattheiss and Warren [15] have presented a band model (based on various crystalline structures) calculation for the electronic structure of expanded liquid mercury and studied the possibility of an energy gap appearing as a result of reduced coordination number. Several other band model calculations [16–18] appeared prior to that of Mattheiss and Warren [15]. All these calculations show clearly a dependence of the critical density at the metal–semiconductor transition on the assumed crystal structure. The calculation by Mattheiss and Warren [15] is probably the most meaningful among the band-model calculations, since the experimental indication [19] is that as a result of increasing temperature the co-ordination number decreases in the liquid, while the average nearest neighbour distance (the position of the first peak in the pair distribution function) stays more or less unchanged. Yonezawa *et al* [20] have employed an effective medium theory together with the single-site approximation to discuss the electronic structure of liquid Hg. Results of the band-model and effective medium calculations are drastically different. Although the band calculation for the crystalline structures comes closer to the experimental results, an improvement in theoretical results based on realistic liquid structure is certainly desirable. Because of a lack of structural models appropriate for higher temperatures, we are unable to address this issue in the present paper. The LMTO (or any other) method based on local density approximation would yield less reliable results as one approaches the transition. A proper way to include the correlation effects near the transition would be warranted. In addition, one would need to go beyond the atomic sphere approximation (ASA) as the structure becomes more open with increasing temperature.

A significant contribution with regard to metal–nonmetal transition in expanded liquid Hg has recently been made by Kresse and Hafner [21]. These authors have used an *ab initio* density functional molecular dynamics simulation to generate liquid Hg structures at higher temperatures and performed a systematic study of the opening of a gap in the single particle DOS with decreasing density. Their calculation reveals the opening of a gap at a density of

about 8.8 g cm^{-3}. Their results suggest that the metal–nonmetal transition is simply a band-crossing transition and that both disorder-induced localization and many-body effects might be less important than had been previously proposed by Cohen and co-workers [22].

The calculations of Kresse and Hafner [21] are based on the $\boldsymbol{k}$-space (supercell) method and use unit cells of 50 atoms. Our calculation is carried out in real space and uses somewhat larger (1372 atoms) clusters. Additional differences come from the choice of the basis, TB-LMTO versus plane waves [21]. The electron–ion interaction in [21] is described by pseudopotentials. By using pseudopotential and plane waves Kresse and Hafner [21] have avoided the problems associated with the LMTO-ASA (atomic sphere approximation) method for open structures. Jank and Hafner [23] have used the LMTO-ASA supercell ($\boldsymbol{k}$-space) method for 64 atom clusters to study the electronic structure of liquid mercury at $-35\,^{\circ}$C. Our study is similar to this calculation in terms of the method (i.e., LMTO) used, but differs in terms of the technique ($\boldsymbol{k}$-space versus real space), cluster size and the temperatures for which the calculation is done ($-35\,^{\circ}$C [23] versus 150–250 $^{\circ}$C). Besides, the clusters used in our calculation and those used by Kresse and Hafner [21] and Jank and Hafner [23] were prepared via different techniques. Since the only comparison between simulated clusters and real systems is via the density and experimental pair distribution functions, it is worthwhile checking whether clusters prepared via different techniques give rise to nontrivial differences in the electronic properties. Finally, both the real-space method and the $\boldsymbol{k}$-space (supercell) method have their advantages and disadvantages. In the $\boldsymbol{k}$-space method one is usually restricted to small clusters and also a small number of $\boldsymbol{k}$-points for computing the energy eigenvalues. But charge self-consistency is achieved for each atom in the cluster. The real-space calculation can be carried out for much larger clusters, but charge self-consistency is achieved on average for a select group of atoms.

The remainder of this paper is divided into the following sections. In section 2 we describe how the model clusters representing liquid mercury were constructed. In section 3 we discuss the electronic structure of liquid and solid mercury. Results for the various crystalline phases are presented in section 3.1, followed by a discussion on the liquid state electronic structure in section 3.2. In section 4 we discuss the resistivity calculation. Section 5 summarizes our results.

2. Simulation of liquid mercury

Clusters representing liquid mercury were generated via the Monte Carlo (MC) method using the well known Metropolis [24] scheme. In order to compare the energies of different configurations a suitable two-body potential was needed. Since there is no suitable pair potential available in the literature for solid or liquid Hg, we attempted to construct one based on a method proposed by Carlsson *et al* [25]†. These authors derived a procedure for inverting the cohesive energy of an isostructural one-component system as a function of volume in order to obtain a pair potential. Essentially, the cohesive energy is written as a lattice sum of some effective two-body potential. The series for the cohesive energy is inverted to obtain the pair potential in the form of a series involving the cohesive energies for various lattice parameters. Suppose that the cohesive energy, E, for nearest neighbour distance r_1 is written as a sum over

† A pair potential for Hg has been discussed by March and co-workers [26]. This potential is derived using the Born–Green approach, and the Kirkwood superposition approximation for the three-body distribution function. The details of this potential in a form suitable for use in a Monte Carlo simulation were not available to us.

the atomic sites $\vec{R}$ of a spherically symmetric and volume-independent pair potential ϕ:

$$E(r_1) = \frac{1}{2N}\sum_{\vec{R}\neq\vec{R}'}\phi(|\vec{R}-\vec{R}'|) \tag{1}$$

$$= \frac{1}{2}\sum_{\vec{R}\neq 0}\phi(|\vec{R}|) \tag{2}$$

$$= \frac{1}{2}\sum_{i} n_i\phi(s_i r_1) \tag{3}$$

where in the final expression the sum is over the various neighbour shells i, containing n_i neighbours at a distance $R_i = s_i r_1$ from the reference atom at the origin. The above series can be inverted to write the pair potential at a distance r as

$$\phi(r) = \frac{2}{n_1}E\left(\frac{r}{s_1}\right) - \sum_{i=2}^{\infty}\left(\frac{2}{n_1}\right)^2\left(\frac{n_i}{2}\right)E\left(\frac{s_i r}{s_1^2}\right) + \sum_{i,j=2}^{\infty}\left(\frac{2}{n_1}\right)^3\left(\frac{n_i}{2}\right)\left(\frac{n_j}{2}\right)E\left(\frac{s_i s_j r}{s_1^3}\right) - \ldots. \tag{4}$$

By including further and further neighbour shells in the sum in equation (4) one can converge to a potential within a given accuracy. However, for the purpose of generating a liquid structure, a rigorous convergence is not necessary. In figure 1(a) we show the potentials in Hg obtained by writing the cohesive energy as a sum of pair potentials involving two and eight shells of neighbours, assuming fcc structure. The difference between the two potentials can be considered as small, in view of the fact that in the MC simulation the pair potential is cut off beyond a certain distance. Usually this is beyond the first minimum in the (experimentally determined) pair distribution function for the liquid structure to be generated. In generating the potentials shown in figure 1 we used the standard LMTO-ASA method to calculate the cohesive energies for various lattice parameters for Hg in the fcc structure using the von Barth and Hedin [27] local density exchange–correlation potential. This choice of the exchange–correlation potential correctly yields the rhombohedral structure ground state energy to be lower than that of other close packed structures such as hcp, fcc and bcc. The calculated ground state (rhombohedral phase) lattice parameter is only $\sim 1\%$ less than the experimental value. The corresponding cohesive energy is 0.84 eV, about 25% higher than the experimental cohesive energy, 0.67 eV. The fcc phase ground state energy is only marginally (about 2%) higher than the rhombohedral phase ground state energy. In our MC simulation we have used the potential obtained by writing the cohesive energy as a sum of pair potentials involving two shells of neighbours in the fcc structure, having fitted this potential to a generalized Morse form:

$$\phi(r) = C(\mathrm{e}^{-2\alpha(r-r_0)} - D\mathrm{e}^{-\alpha(r-r_0)}) \tag{5}$$

with $C = 0.183\,43$ eV, $\alpha = 1.8537$ Å^{-1}, $r_0 = 3.1366$ Å, $D = 1.6877$. The potential was cut off beyond 4.5 Å. In figure 1(b) we compare the potential obtained from the cohesive energy (fitted to equation (4) with two shells of neighbours) with that given by the analytic form given by equation (5). As discussed in detail by Carlsson *et al* [25], the depth of the potential thus obtained is too large compared with the potentials obtained by the pseudopotential approach (for sp-bonded metals) or by fitting to experimental cohesive energy and other elastic properties. For example, the potential given by equation (5) has a depth of 0.128 eV, whereas the melting point of Hg is 233 K or 0.02 eV. The simulation using the above potential had to be carried out at a very high temperature (above 3000 K) to obtain pair distribution functions that match

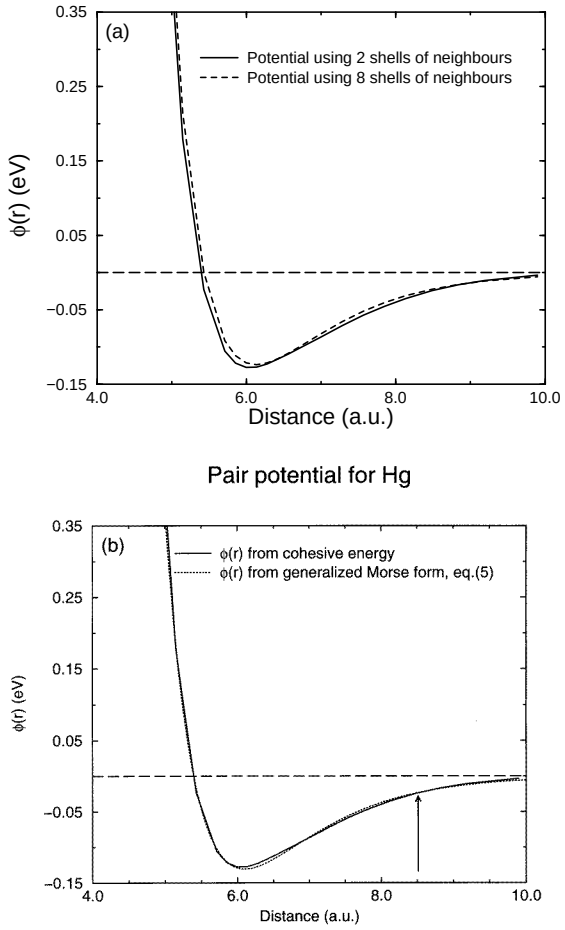

Figure 1. (a) Pair potentials for Hg obtained by writing the cohesive energy as a sum of two and eight shells of neighbours in the fcc phase, and by using equation (4), (b) pair potential obtained by writing the cohesive energy as a sum of two shells of neighbours in the fcc phase, compared with that given by the generalized Morse potential, equation (5). The arrow indicates the location of the cut-off in the potential for the MC simulation.

the experimental curves in the temperature range 150–250 °C (Waseda 1980 [28]). In the context of the present work the simulation temperature has no physical significance beyond simply a means of generating liquid clusters via a canonical MC simulation. In figure 2 we compare the pair distribution functions of 1372 atom clusters obtained via simulations with the experimental distributions at 150 °C and 250 °C. The number densities of these clusters are chosen to be the appropriate values for the corresponding temperatures (0.0386 $Å^{-3}$ at 250 °C, and 0.0397 $Å^{-3}$ at 150 °C [28]). The agreement between the experimental and the simulated pair distribution functions is excellent at 250 °C and becomes poorer for lower temperatures. However, for 150 °C the agreement is still good enough to permit the use of the simulated clusters as appropriate models for liquid Hg at 150 °C. In figure 3(a) we compare the experimental pair distribution functions [28] of liquid Hg at −35 °C and 250 °C. There are nonsignificant differences in the two pair distributions, especially beyond the first peak, which cannot be reproduced via the volume-independent pair potential we have used for the

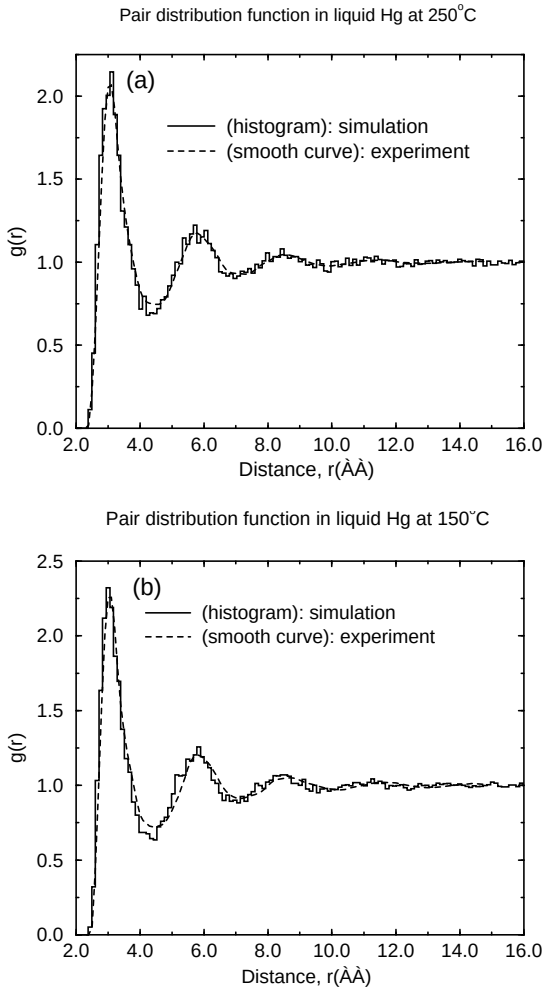

Figure 2. Pair distribution functions in simulated clusters for liquid Hg compared with the corresponding experimental results [28], for (a) 250 °C and (b) 150 °C.

simulation. In part (b) of this figure we have plotted our best simulation result for −35 °C with the corresponding experimental curve. It is possible to fit the first peak in the experimental curve to the simulation result, but agreement beyond the first peak stays poor. Tamura and Hosokawa [29] have presented x-ray diffraction measurements of expanded fluid Hg up to the supercritical region. The pair distribution function shows very little change between 250 and 500 °C, apart from a slight broadening of the first peak with increasing temperature. The density decreases from 12.98 g cm^{-3} to 12.40 g cm^{-3}. Hence we expect the electronic structure to change very little between 250 and 500 °C. The results that we present in this paper (based on our clusters representing liquid Hg at 250 °C) can be considered to be representative of liquid Hg between 250 and 500 °C. In the absence of an appropriate volume-dependent two-body potential we have decided not to extend our study to higher temperatures at this stage.

Potentials constructed via nonlocal exchange–correlation functionals differ somewhat from those obtained with local functionals in terms of the depth and the location of the minimum. For example, the exchange–correlation potential by Perdew and Wang [30] gives the

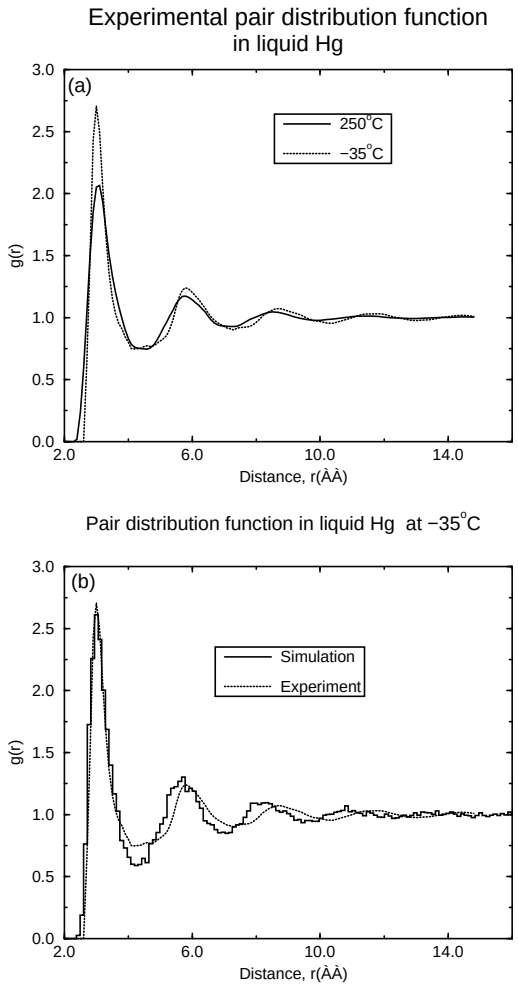

Figure 3. (a) Experimental pair distribution functions in liquid Hg at −35 °C and 250 °C [28], (b) pair distribution function in liquid Hg at −35 °C [28] compared with that of a simulated cluster, indicating lack of agreement beyond the first peak.

fcc structure as the lowest energy one and the cohesive energies for various lattice parameters for this structure then yield a pair potential, which can be parametrized as

$$\phi(r) = \frac{A_6}{d^6} + \frac{A_4}{d^4} + \frac{A_3}{d^3} + \frac{A_2}{d^2} + \frac{A_1}{d} + A_0 \tag{6}$$

where $d = r^2$, and $A_6 = 1346.9077$ eV/Å^{12}, $A_4 = 5356.56$ eV/Å^8, $A_3 = -630.394$ eV/Å^6, $A_2 = 22.0034$ eV/Å^4, $A_1 = -1.4984$ eV/Å^2, $A_0 = 0.062\,313$ eV. MC simulations using this potential at temperatures around 3000 K yield clusters with pair distribution functions very similar to those shown in figure 2.

Recently, Munejiri *et al* [31] have used the 'inverse method' to generate an effective pair potential $\phi(r)$ for mercury. The method is based on a combination of integral equations and computer simulations. The integral equations used connect $\phi(r)$ to the experimental radial distribution function, the direct correlation function as well as the so-called bridge function. A molecular dynamics simulation is performed with an initial choice of the bridge function

appropriate for a hard sphere system. The radial distribution function and the corresponding structure factor are calculated for the simulated clusters. These are used to update the direct correlation function and the bridge function. The new $\phi(r)$ obtained from these updated quantities is used in the simulation to generate new clusters and the process is iterated until convergence to desired accuracy is obtained in $\phi(r)$. We are currently exploring this method as well as the reverse Monte Carlo method of Reevy *et al* [32]. Both of these methods are considerably more demanding of computer time than the Metropolis Monte Carlo method used in this work.

3. Electronic structure

By now the LMTO and TB-LMTO methods are well documented [11, 12] well tested schemes, and have been used extensively (see, e.g., [33–36]) in the study of all forms of condensed matter: periodic, quasiperiodic and disordered. We use the standard LMTO method to study the electronic structure of the crystalline phases and the TB-LMTO scheme to study the liquid phase. We have used both the first-order TB-LMTO Hamiltonian H_1 (Hamiltonian in the most localized, but nonorthogonal basis) as well as the second-order Hamiltonian H_2 (less localized, but nearly orthogonal basis). Recursion calculation using the second-order Hamiltonian H_2 was carried out using the approximations described in earlier publications [33–36].

3.1. Crystalline phases

The standard scalar-relativistic LMTO-ASA method, including combined corrections, was used to determine the electronic structure of Hg in the assumed crystalline phases: fcc, rhombohedral, hcp, bcc and diamond. It was found that the use of a local density exchange–correlation functional such as that due to von Barth and Hedin [27] or Vosko, Wilk and Nusair [37] yields correctly the rhombohedral phase as the ground state crystal structure, although the lattice parameter is underestimated by about 1% and the cohesive energy is overestimated by 10–15%, with respect to the corresponding experimental values. The agreement for the lattice parameter can perhaps be improved by going beyond the ASA, i.e., using the full-potential LMTO method. The use of the modified gradient expansion approximation of Langreth, Mehl and Hu (Langreth and Mehl [38]; Hu and Langreth [39]) overestimates the ground state lattice parameter by about 2% compared with the experimental value.

In figure 4 we show the DOS in the close-packed structures: rhombohedral, fcc and hcp, obtained by using the von Barth and Hedin [27] exchange–correlation potential. The DOS shown are for Wigner–Seitz (W–S) radius (radius of space filling spheres centred about the atoms) $W = 3.3334$ au. This is the W–S radius for the experimental rhombohedral ground state of Hg, corresponding to a density of approximately 14.5 g cm^{-3}. The values of W corresponding to the lowest energy, for the von Barth and Hedin [27] exchange–correlation potential, are 3.3124 au, 3.3334 au, and 3.3034 au for the fcc, hcp and rhombohedral structures, respectively, with the rhombohedral structure giving the lowest energy among all the structures studied. Even at $W = 3.3334$ au the rhombohedral phase energy is lower than that for the other structures. The lowering of energy in going from the fcc to the rhombohedral phase is due to slightly enhanced s–p hybridization in the rhombohedral phase, leading to an increased number of p electrons, and making the charge distribution more 'covalent-like'. This point was discussed recently by Singh [40], who studied the importance of relativistic effects in determining the cohesive properties of Hg. It is noteworthy that although the rhombohedral phase is the lowest energy one, the corresponding DOS does not show any noticeable pseudogap at the Fermi energy E_F. One can conclude that for close-packed structures the pseudogap is

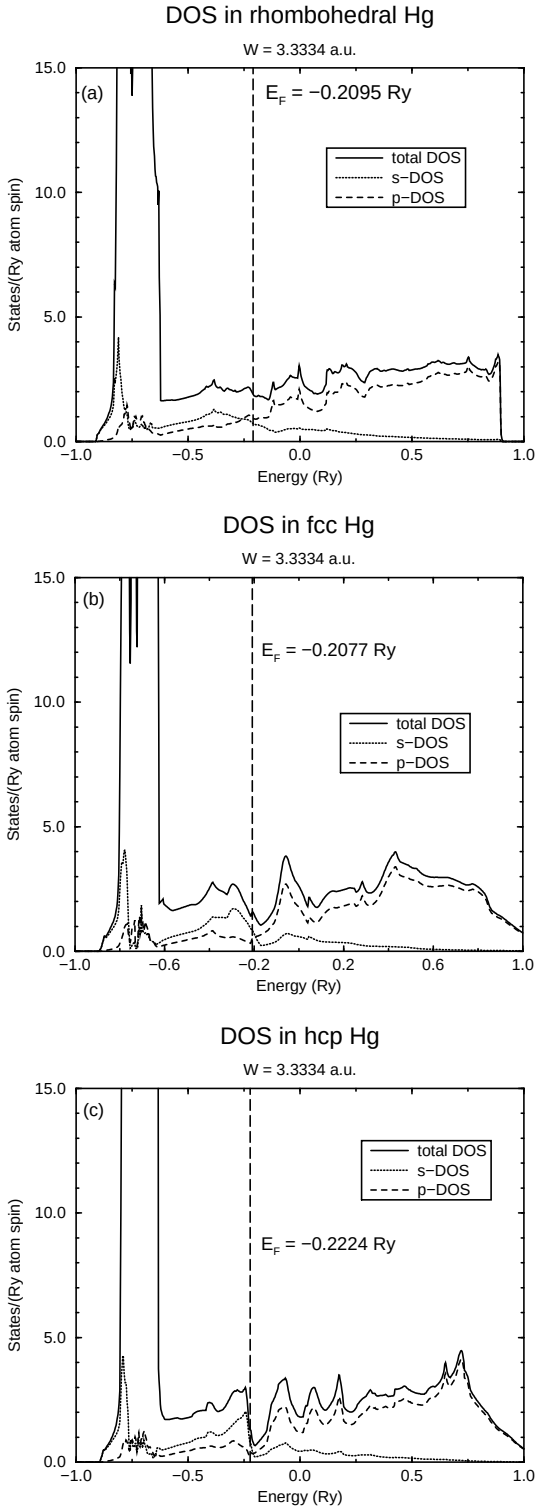

Figure 4. DOS for Hg in various assumed crystalline phases: (a) rhombohedral, (b) fcc and (c) hcp. See text for details. Vertical lines show the locations of the Fermi energy.

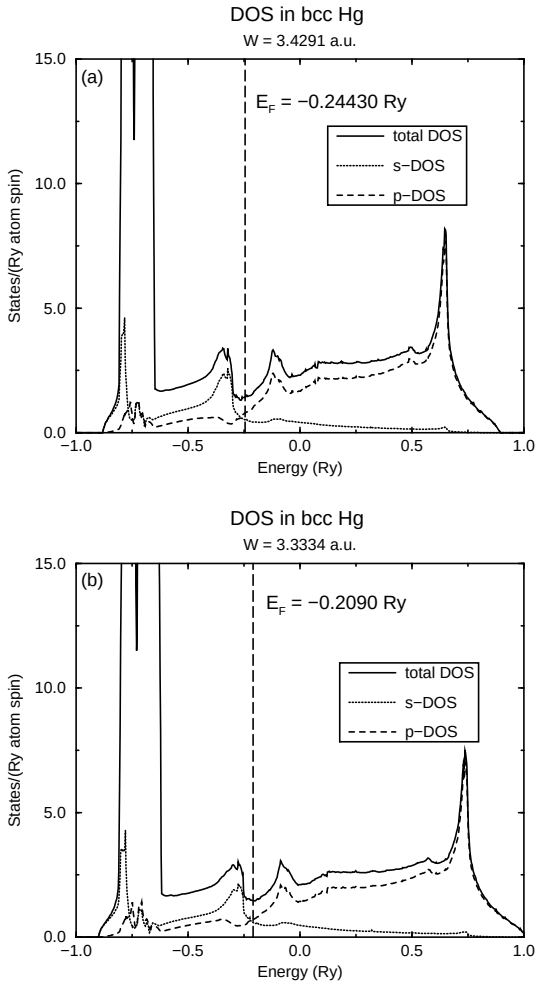

Figure 5. DOS for Hg in bcc structure. See text for details. Vertical lines show the locations of the Fermi energy.

quite sensitive to the exact arrangement of neighbours.

In figure 5 we show the DOS for the less close-packed bcc structure for two values of W–S radius: $W = 3.3334$ au and $W = 3.4291$ au. The latter value of W corresponds to the same nearest neighbour distance as in the close-packed structures considered in figure 4 (corresponding to a density of 13.3 g cm^{-3}). The lowest energy for the bcc phase is obtained for $W = 3.3334$ au. Note that for $W = 3.4291$ au the width of the pseudogap at E_F is larger than that for the hcp and fcc structures shown in figure 4. For $W = 3.3334$ au the decrease in the nearest neighbour distance leads to increased overlap between neighbouring orbitals and the pseudogap is somewhat reduced. But even at this decreased nearest neighbour distance the width of the pseudogap is larger than that in fcc or hcp phase.

The results for the crystalline structure reveal the importance of reduced coordination number in producing or enhancing the pseudogap near the Fermi level. It should be noted that in a low co-ordination environment the pseudogap is more stable against small fluctuations in positions of near neighbours than in close-packed environments. This is because for close-

packed configurations small changes in the nearest neighbour positions can render the structure from fcc-like to rhombohedral-like, causing a noticeable change in the magnitude of the pseudogap. Note that for the same density or W–S radius ($W = 3.3334$ au) the fcc structure has a pronounced pseudogap (figure 4(b)), whereas for the rhombohedral structure no such feature is noticeable (figure 4(a)). For less close-packed structures the pseudogap is wider, making it less sensitive to the exact arrangement of near neighbours. Our calculations for the diamond structure also support this conclusion. This conclusion, based on our calculations for the ground state nearest neighbour distance, should hold qualitatively at higher temperatures for increased nearest neighbour distance. At higher temperatures the reduced average coordination may play a more pivotal role in determining the pseudogap at the Fermi energy than increased near neighbour separation.

3.2. Liquid phase

In figure 6 we show the DOS calculated for fcc Hg at a density of 0.0386 atoms Å^{-3}, the density of liquid Hg at 250 °C [28], using the standard LMTO method and the recursion method [13] applied to a 1372 atom fcc cluster with periodic boundary conditions. The second-order Hamiltonian H_2 was used for the recursion method calculation and the continued fraction was terminated using the linear predictor method of Allan [41]. The difference in the band widths in the two calculations is due to the differences in the Hamiltonians used, H_2 being only the first two terms in the infinite series on the rhs of equation (3) representing the full LMTO-ASA Hamiltonian. Both DOS show a pseudogap with the Fermi energy (E_F) lying slightly above the minimum of the pseudogap. The similarity of the two curves shows the reliability of the real space method we are going to use for calculating the liquid state electronic structure and also that features such as a deep minimum in the DOS (i.e., pseudogap) are reproducible via the recursion method.

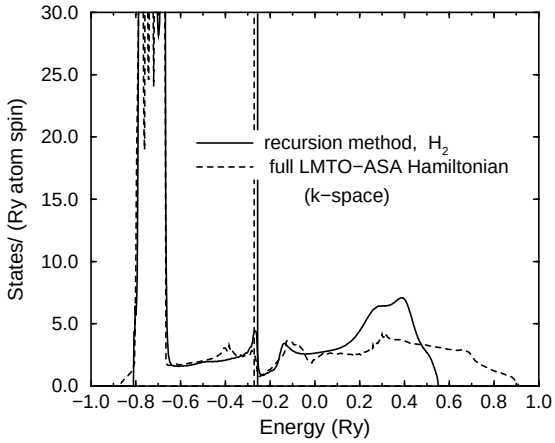

Figure 6. The DOS for fcc Hg at the density of liquid Hg at 250 °C, calculated via the standard LMTO-ASA (***k***-space) method and the recursion method using Hamiltonian H_2. Vertical lines show the locations of the Fermi energy.

As discussed towards the end of section 2, although H_1 is the Hamiltonian in the most localized TB-LMTO basis, the DOS calculated from H_1 using the standard orthogonal recursion scheme may not be accurate, because of the nonorthogonality of the corresponding TB-LMTO basis. To incorporate the effect of the nonorthogonality of the basis one can carry

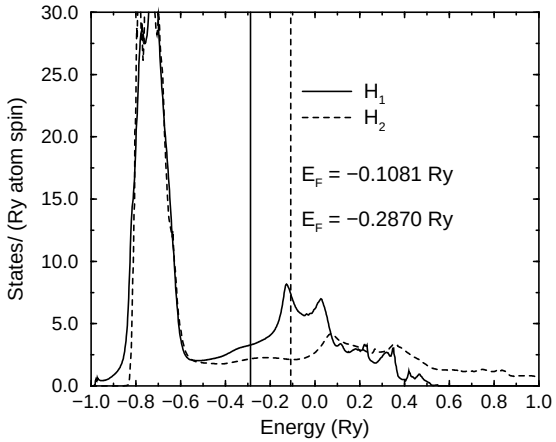

Figure 7. A comparison of the DOSs in liquid Hg at 250 °C, calculated by using the Hamiltonians H_2 and H_1. Each DOS is a ten atom average in a 1372 atom cluster. Vertical lines show the locations of the Fermi energy.

out the recursion using the Hamiltonian H_2. In figure 7 we display the DOS calculated with the Hamiltonians H_2 and H_1 for a 1372 atom cluster representing liquid Hg at 250 °C. The DOS shown are ten atom averages. The effect of the second term on the rhs of equation (3) is to shift most energy eigenvalues to higher energy, increasing the bandwidth as well as pushing the bottom of the band to higher energy compared with the TB-LMTO Hamiltonian H_1. The shape of the DOS around the Fermi energy E_F (between -0.3–0.0 Ryd) is given more correctly by H_2 than by H_1. In the d part of the band, both H_2 and H_1 give more or less the same DOS. Note that the value of $N(E_F)$, the DOS at the E_F, is about 30% smaller for H_2.

To ensure that the features in the density of states are not influenced by the particular terminator used for the recursion method, we have repeated the calculation with several different schemes of terminating the continued fraction. None of the methods used showed any evidence of a pseudogap for the liquid state density of states. In figure 8 we present the DOS (ten atom average) in a liquid Hg cluster for 250 °C obtained by using the Allan terminator [41] and that due to Beer and Pettifor [42]. The DOS shown are for the Hamiltonian H_1 and the similarity of the two DOS clearly indicates that our results are independent of the particular method of terminating the continued fraction expansion of the Green function.

In figure 9 we show the DOS for 1372 atom clusters representing liquid Hg at 250 and 150 °C, obtained by using the Hamiltonian H_2. Each DOS shown is an average over the local DOS for 100 atoms in the cluster, and the terminator used is that due to Allan [41]. The calculated DOS at the Fermi level shows a lowering with respect to the free electron DOS and the Mott g-factor is approximately 70% (71.4% at 250 °C). This agrees well with the result of electron spectroscopy studies of Oelhafen *et al* [10]. However, a deep pseudogap as observed in most crystalline phases (fcc, bcc, diamond and hcp) does not exist in the liquid state around the temperatures 150–250 °C. The pronounced pseudogap of the crystalline phase disappears in the liquid phase due to fluctuations in local environments causing local '6s' and '6p' DOS to vary somewhat in their peak heights, centres and widths. In figure 10 we show the local s and p orbital projected DOS for ten different atoms in a cluster representing liquid Hg at 250 °C. The variations in their magnitude at the Fermi level are large enough to wipe out a pseudogap-like feature in this energy region. Based on the results for the crystalline phase DOS we can understand that this is due to the fact that at temperatures $\sim$ 500 °C the liquid

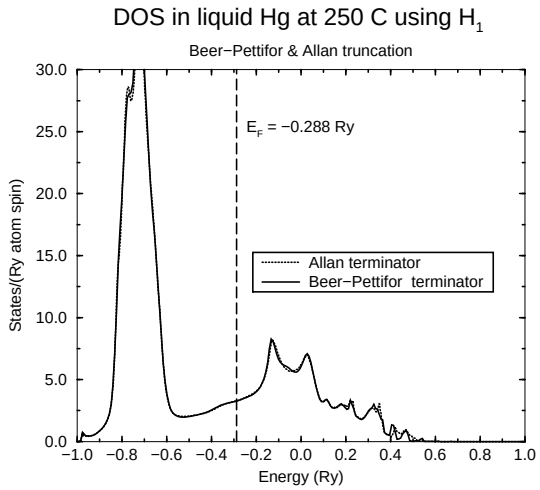

Figure 8. DOS in a 1372 atom cluster representing liquid Hg at 250 °C using the Allan [41] and Beer and Pettifor [42] terminators. The vertical line shows the location of the Fermi energy.

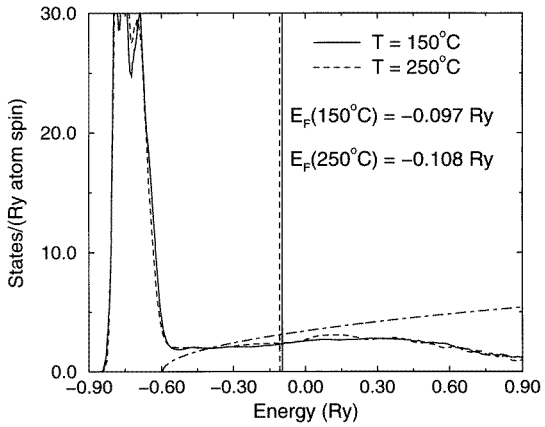

Figure 9. The DOS in liquid Hg at 250 °C and 150 °C calculated via the recursion method using Hamiltonian H_2. Results show 100 atom averages. Vertical lines show the locations of the Fermi energy. The free electron DOS is also shown.

structure is more or less close packed, the number of atoms within the first peak in the pair distribution function being around ten. It is expected that at higher temperatures the pseudogap should reappear and become deeper as a result of decreasing co-ordination number leading to less overlap of s and p orbitals. The latter reduces the width of both s and p bands, and the hybridization between them. According to the calculation of Kresse and Hafner [21] this pseudogap due to increased separation of s and p bands appears in the liquid state at the density of 8.8 g cm^{-3}.

The agreement between our results and that of Hafner and co-workers [21, 23] is good. Small differences in results are primarily due to differences in the densities considered. Kresse and Hafner [21] report electronic structure for densities 12.40 g cm^{-3} and above for liquid Hg, while Jank and Hafner [23] report the results for 13.6 g cm^{-3}. The densities of our liquid

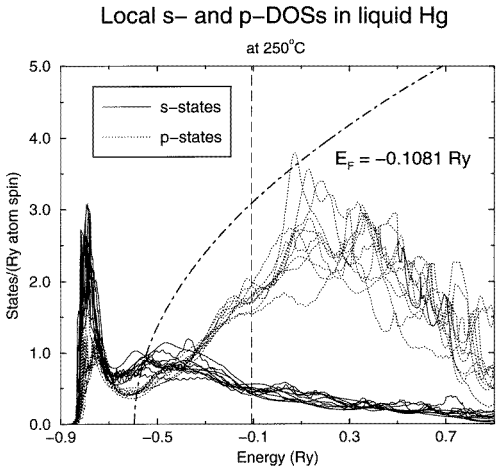

Figure 10. Local s- and p-orbital projected DOS shown for ten atoms in a 1372 atom cluster representing liquid Hg at 250 °C. The vertical line shows the location of the Fermi energy. The free electron DOS is also shown.

clusters, appropriate for 250 °C and 150 °C, are 12.86 g cm^{-3} and 13.23 g cm^{-3}, respectively. The shape, valence band width and the value of the DOS at the Fermi level in our calculation and that of Hafner and co-workers [21, 23] are all similar. Both ours and the calculations of [21] and [23] show a similar lowering of the DOS below the free electron value. The appearance of a minimum in the DOS starts around a density of 12.40 g cm^{-3} [21]. The minimum liquid density considered by us is 12.86 g cm^{-3}.

In figure 11(a) we show the average s- and p-orbital projected DOS in liquid Hg at 250 °C. In figure 11(b) we compare the s- and p-orbital projected DOS in liquid Hg clusters at 250 and 150 °C. The minimum occurring in the s,p DOS at energies below E_F is not due to increased separation between the centres of the 6s and 6p bands, but due to the hybridization of the d band with the sp band, sometimes referred to as a 'Fano effect'. As shown in figure 9, apart from an almost imperceptible decrease in the d bandwidth there is virtually no change in the DOS as the temperature increases from 150 °C to 250 °C, the DOS at E_F remaining around [2–2.2] states/(Ryd atom), not much different from that in the rhombohedral ground state of Hg. Both s and p DOS at the Fermi energy are found to remain unchanged in our calculation as the temperature increases from 150 °C to 250 °C. The lack of variation in the s DOS is in agreement with the measurement of the Knight shift in liquid Hg, which is found to be more or less independent of the density around these values [15].

Based on their electron spectroscopy studies, Oelhafen *et al* [10] remark that the minimum in the DOS at the Fermi level can be observed only in the liquid state and not in the solid state at −183 °C. Our calculations show (figures 4 and 5) that although the pseudogap is present in several crystalline phases (fcc, bcc, hcp and diamond), it is nonexistent in the rhombohedral phase (density equal to 14.5 g cm^{-3}), which is the ground state, according to our total energy calculations. According to our calculations the Mott g-factor is about 10% lower in the liquid phase at 250 °C than in the rhombohedral ground state. This result is in consistence with the above remark by Oelhafen *et al* [10]. For Hg the spin–orbit interaction should lead to a splitting of the 5d band into 5d$^{3/2}$ and 5d$^{5/2}$ bands. Our scalar-relativistic calculation neglects the spin–orbit interaction. Oelhafen *et al* [10] mention that their measurements clearly show that only the 5d$^{5/2}$ electrons hybridize with the 6s electrons, while 5d$^{3/2}$ electrons strictly

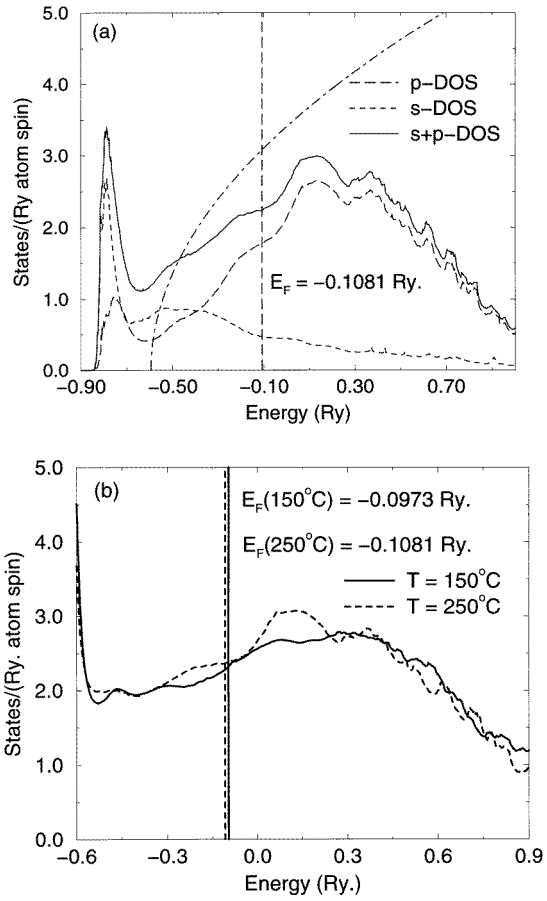

Figure 11. s- and p-orbital projected DOSs in liquid Hg: (a) at 250 °C (the free electron DOS is also shown), (b) total s+p DOS compared at 250 °C and 150 °C. Vertical lines show the locations of the Fermi energy.

preserve their core character. Clearly, a better agreement with experiment would warrant a fully relativistic calculation, also perhaps going beyond the local density approximation used in the present work.

For the sake of completeness we also include (figure 12) the DOS for the liquid cluster at −35 °C. Overall features of this DOS are almost identical to that for 250 °C. Since the pair distribution for this cluster agrees with the experimental curve only up to the first peak, the DOS shown in figure 12 is less reliable than the DOS shown for 150 °C and 250 °C.

4. Electrical conductivity

We have calculated the resistivity of the liquid clusters using the Kubo–Greenwood formula [14] and the TB-LMTO-recursion method, as discussed by Bose, Jepsen and Andersen [36]. According to the Kubo–Greenwood formula the diagonal elements of the zero-temperature dc

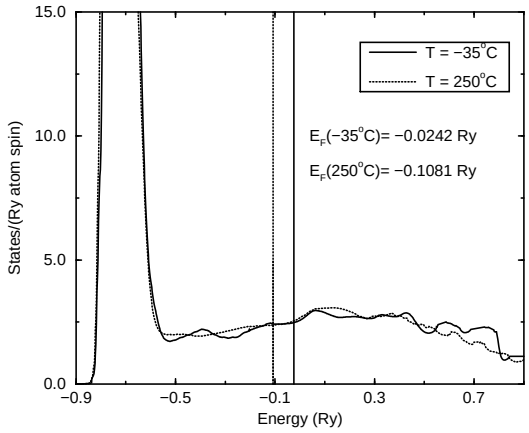

Figure 12. The DOS of a 1372 atom cluster representing liquid Hg at −35 °C. Vertical lines show the locations of the Fermi energy.

conductivity tensor in the eigenfunction representation are given by

$$\sigma_{jj} = \frac{e^2 h}{\Omega} \sum_{m,n} |\langle E_m | v_j | E_n \rangle|^2 \delta(E_m - E_F)\delta(E_n - E_F) \tag{7}$$

where Ω is the sample volume, h is Planck's constant, E_F is the Fermi energy and v_j is the j component of the velocity operator. Relating the Dirac-δ function to the imaginary part of the Green function and using the expression

$$\sum_m \delta(E - E_m)\langle E_m | f(E) | E_m \rangle = g(E)\overline{f(E)}_{E_m = E} \tag{8}$$

where the bar implies an average over the eigenfunctions with energy E, and $g(E)$ is the sample DOS at energy E, equation (10) can be put in a physically transparent form:

$$\sigma_{jj} = \frac{e^2}{\Omega_a} n(E_F) D(E_F). \tag{9}$$

Here Ω_a is the volume per atom, $n(E_F)$ is the DOS per atom at the Fermi energy and $D(E_F)$ is the diffusivity given by

$$D(E_F) = -\overline{h} \lim_{\epsilon \to 0^+} \mathrm{Im}[\overline{\langle E_m | v_j G(E_F + \mathrm{i}\epsilon) v_j | E_m \rangle}]_{E_m = E_F}. \tag{10}$$

Apart from a numerical factor, $D(E_F)$ can be considered as the average local DOS projected onto the states $v_j|E_m\rangle$, and this we calculate using the recursion method. We calculate the eigenvectors $|E_m\rangle$ by a filtering technique used originally by Kramer and Weaire [43]. The matrix elements of the velocity operator in the TB-LMTO basis are

$$(v_j)_{\beta\gamma} = \left(\frac{\mathrm{i}}{\overline{h}}\right) \sum_{\delta} (H_{\beta\delta} x^j_{\delta\gamma} - x^j_{\beta\delta} H_{\delta\gamma}) \tag{11}$$

where x and H denote the position and the Hamiltonian operators and the subscripts denote the combined angular momentum and the site indices. The matrix elements of the position operator, $x^j_{\gamma\beta}$, can be written as

$$x^j_{\gamma\beta} = \langle \chi^\alpha_\gamma | x^j | \chi^\alpha_\beta \rangle = \frac{1}{2}(x^j_\gamma + x^j_\beta) O^\alpha_{\gamma\beta} + \langle \chi^\alpha_\gamma | \left[x^j - \frac{1}{2}(x^j_\gamma + x^j_\beta) \right] | \chi^\alpha_\beta \rangle \tag{12}$$

where x^j_β is the x^j coordinate of the atomic nucleus on which the orbital β is centered. $|\chi^\alpha_\beta\rangle$ represents a TB-LMTO orbital with the subscript denoting jointly a site and the collective angular momentum index L. The second term on the rhs of the above equation, the so-called dipole term, is neglected. If the diffusivity calculation is carried out by using the Hamiltonian H_2, then the nonorthogonality of the basis is small and can be neglected. For calculations involving H_1 the overlap matrix $O^\alpha_{\gamma\beta}$ must be included in the computation of the matrix elements of the position operator.

Resistivity calculations for the 1372-atom liquid Hg clusters were carried out using the Hamiltonian H_2. The overlap matrix in equation (12) was replaced by the identity matrix. The calculated value for liquid Hg at 250 °C was approximately 200 $\mu\Omega$ cm. The resistivities for the clusters representative of -35 °C and 150 °C were close to this value, being within the error bars of the computed values, $\pm 15\ \mu\Omega$ cm. This is because the structural differences between the clusters is small and we have used the zero temperature Kubo–Greenwood formula, neglecting the Fermi factor. The measured resistivity values at 100 °C and 500 °C are 103.3 $\mu\Omega$ cm and 160 $\mu\Omega$ cm, respectively [44]. The present calculation indicates the effectiveness of the TB-LMTO-recursion scheme for the study of electronic transport in systems such as liquid Hg, but stands in need of further improvement.

The most noteworthy source of error in the resistivity calculation as described above is the approximate treatment of the velocity matrix elements. The neglect of the dipole term in equation (12) can be justified if the basis consists of only s and d orbitals, with pure s and d symmetry. The inclusion of the p orbitals in the basis, as well as the fact that the TB-LMTO orbitals lack pure angular momentum (L) symmetry, makes the validity of this approximation questionable. Apart from this, there are possible errors associated with the recursion method, and inadequacies in structural models. It is also important to check the saturation in the computed resistivity value with the cluster length. This involves preparing clusters of different lengths, and was not done in the present work.

5. Comments and conclusions

We have presented the electronic DOS for realistic structural models of liquid mercury in the temperature range 150–250 °C. Our calculation does not yield any noticeable local minimum near the Fermi level. However, a lowering of the DOS at the Fermi level with respect to the free electron value is observed and the magnitude of the Mott g-factor ($\sim$70%) agrees with the results obtained by Hafner and co-workers [21, 23] as well as the photoemission studies by Oelhafen *et al* [10]. The calculations for various assumed crystalline phases of Hg reveal the importance of reduced coordination number in the opening of a pseudogap. It is found that in the bcc structure the pseudogap is quite stable against changes in the near neighbour distance. In close packed structures like fcc, hcp and rhombohedral the pseudogap is sensitive to the details of the near neighbour arrangements. It is thus conceivable that in liquid Hg at high temperatures, where the average coordination number becomes bcc-like or less, a pseudogap (in the sense of a pronounced local minimum in the DOS) at the Fermi level exists. Recently, Nield and Verronen [45] have studied the structure of expanded liquid mercury by applying the reverse Monte Carlo modelling technique to the x-ray diffraction data of Tamura and Hosokawa [29]. The calculated value of the coordination number depends on the method used to evaluate this quantity, and error bars of ± 2 are common. However, the elaborate study of Nield and Verronen [45] suggests that an average coordination number of less than eight can appear in liquid Hg for densities less than 9.24 g cm^{-3} or for temperatures higher than 1400 °C. For temperatures up to $\sim$ 500 °C, where the structure is more or less close packed, fluctuations in local environments are expected to prevent the formation of any deep local

minimum. This observation is supported by the theoretical work of Hafner and co-workers [21, 23]. The absence of a deep local minimum in the DOS as seen in this work is in agreement with the earlier work by Chan and Ballentine [3] and with the observations made by Ballentine [6] in his review article. No pronounced local minimum near E_F accompanies the lowering of the DOS below the free electron value in liquid Hg at temperatures below $\sim 500\ ^\circ$C.

Resistivity calculation, based on the Kubo–Greenwood formula and TB-LMTO-recursion method, yields values for the liquid Hg clusters that are similar to the experimental values. Calculations based on realistic structural models and equations (9)–(12) can provide insight into the decrease in resistivity of liquid Hg on alloying. For example, in Hg–In the volume per atom Ω_a should be slightly higher than that in pure liquid Hg (see tables on pages 270–273 of [28]). This would increase resistivity. However, $n(E_F)$ might increase as a result of hybridization, and if the weight of the s states at the Fermi level increases on alloying, the diffusivity $D(E_F)$ might also increase, resulting in an overall increase in conductivity. We are currently in the process of generating alloy structures to be able to carry out such calculations.

Acknowledgments

This work was supported by the Natural Sciences and Engineering Research Council of Canada. The author would like to thank Professor O K Andersen for his hospitality at the Max-Planck-Institute of Solid State Research, Stuttgart, Germany, where a part of this work was carried out. Helpful discussions with O K Andersen and O Jepsen are gratefully acknowledged. Finally, a sincere 'thank you' to the referee who brought the important work of Hafner and co-workers [21, 23] to the author's attention.

References

[1] Mott N F 1966 *Phil. Mag.* **13** 989
[2] Evans R 1970 *J. Phys. C: Met. Phys. Suppl.* **2** S137
[3] Chan T and Ballentine L E 1971 *Phys. Lett.* A **35** 385
Chan T and Ballentine L E 1972 *Can. J. Phys.* **50** 813
[4] Jones J C and Datars W R 1971 *J. Phys. F: Met. Phys.* **1** L56
Jones J C and Datars W R 1972 *Can. J. Phys.* **50** 1659
[5] Itami T and Shimoji M 1972 *Phil. Mag.* **25** 229
[6] Ballentine L E 1975 *Adv. Chem. Phys.* **31** 263
[7] Mott N F 1972 *Phil. Mag.* **26** 505
[8] Norris C, Rodway D C and Williams G P 1973 *The Properties of Liquid Metals Proc. 2nd Int. Conf. (Tokyo, 1972)* ed S Takeuchi (London: Taylor and Francis) p 181
[9] Cotti P, Güntherodt H-J, Munz P, Oellhafen P and Wullschleger J 1973 *Solid State Commun.* **12** 635
[10] Oelhafen P, Indlekofer G and Güntherodt H-J 1988 *Z. Phys. Chem., NF* **157** 483
[11] Andersen O K and Jepsen O 1984 *Phys. Rev. Lett.* **53** 2571
[12] Andersen O K, Jepsen O and Glötzel D 1985 *Highlights of Condensed Matter Theory* ed F Bassani, F Fumi and M P Tosi (Amsterdam: North-Holland) pp 59–176
[13] Haydock R 1980 *Solid State Physics: Advances in Research and Applications* vol 35, ed F Seitz and D Turnbull (New York: Academic) pp 215–94; see also articles by V Heine and M J Kelly in the same volume
[14] Kubo R 1956 *Can. J. Phys.* **34** 1274
Greenwood D 1958 *Proc. Phys. Soc., London* **71** 585
[15] Mattheiss L F and Warren W W Jr 1977 *Phys. Rev.* B **16** 624
[16] Devillers M A C and Ross R G 1975 *J. Phys. F: Met. Phys.* **5** 73
[17] Overhof H, Uchtmann H and Hensel F 1976 *J. Phys. F: Met. Phys.* **6** 523
[18] Fritzson P and Berggren K-F 1976 *Solid State Commun.* **19** 385
[19] Waseda Y, Yokoyama K and Suzuki K 1974 *Phil. Mag.* **29** 1427
[20] Yonezawa F and Martino F 1976 *Solid State Commun.* **18** 1471

Yonezawa F, Martino F and Asano S 1977 *Liquid Metals, 1976* ed R Evans and D A Greenwood (Bristol: Institute of Physics)
[21] Kresse G and Hafner J 1997 *Phys. Rev.* B **55** 7539
[22] Cohen M H and Jortner J 1973 *Phys. Rev. Lett.* **30** 696
Cohen M H and Jortner J 1974 *Phys. Rev.* A **10** 978
Turkevich L A and Cohen M H 1984 *Phys. Rev. Lett.* **53** 2323
[23] Jank W and Hafner J 1990 *Phys. Rev.* B **42** 6926
Jank W and Hafner J 1990 *J. Non-Cryst. Solids* **117/118** 304
[24] Metropolis N, Rosenbluth A W, Rosenbluth M N, Teller A H and Teller E 1953 *J. Chem. Phys.* **21** 1087
[25] Carlsson A E, Gelatt C D Jr and Ehrenreich H 1980 *Phil. Mag.* A **41** 241
[26] Johnson M D and March N H 1963 *Phys. Lett.* **3** 313
Worster J and March N H 1964 *Solid State Commun.* **2** 245
[27] von Barth U and Hedin L 1972 *J. Phys. C: Solid State Phys.* **5** 1629
[28] Waseda Y 1980 *The Structure of Non-Crystalline Materials* (New York: McGraw-Hill) pp 272–3
[29] Tamura K and Hosokawa S 1992 *J. Non-Cryst. Solids* **150** 29
Tamura K and Hosokawa S 1993 *J. Non-Cryst. Solids* **156–158** 646
Tamura K and Hosokawa S 1994 *J. Phys.: Condens. Matter.* **6** A241
[30] Perdew J P and Wang Y 1986 *Phys. Rev.* B **33** 8800
[31] Munejiri S, Shimojo F and Hoshino K 1998 *J. Phys.: Condens. Matter* **10** 4963
[32] McGreevy R L, Howe M A, Keen D A and Clausen K N 1990 *Neutron Scattering Data Analysis (Inst. Phys. Conf. Ser. 107)* (Bristol: Institute of Physics) p 165
McGreevy R L and Pusztai L 1990 *Proc. R. Soc.* A **430** 241
McGreevy R L and Pusztai L 1988 *Mol. Sim.* **1** 359
[33] Bose S K 1998 *Metall. Mater. Trans.* A **29** 1853
[34] Bose S K, Jaswal S S, Andersen O K and Hafner J 1988 *Phys. Rev.* B **37** 9955
[35] Bose S K, Kudrnovský J, Mazin I I and Andersen O K 1990 *Phys. Rev.* B **41** 7988
[36] Bose S K, Jepsen O and Andersen O K 1993 *Phys. Rev.* B **48** 4265
[37] Vosko S H, Wilk L and Nusair M 1980 *Can. J. Phys.* **58** 1200
[38] Langreth D C and Mehl M J 1981 *Phys. Rev. Lett.* **47** 446
Langreth D C and Mehl M J 1983 *Phys. Rev.* B **28** 1809
[39] Hu C D and Langreth D C 1985 *Phys. Scr.* **32** 391
[40] Singh P P 1994 *Phys. Rev. Lett.* **72** 2446
[41] Allan G 1984 *J. Phys. C: Solid State Phys.* **17** 3954
Allan G 1985 *The Recursion Method and its Applications (Springer Series in Solid State Sciences 58)* ed D G Pettifor and D L Weaire (Berlin: Springer) pp 61–9
[42] Beer N and Pettifor D G 1984 *Electronic Structure of Complex Systems* ed P Phariseau and W M Temmerman (New York: Plenum) p 769
[43] Kramer B and Weaire D 1978 *J. Phys. C: Solid State Phys.* **11** L5
[44] Smithells C J (ed) 1976 *Metals Reference Book* 5th edn (London: Butterworths) p 947
[45] Nield V M and Verronen P T 1998 *J. Phys.: Condens. Matter* **10** 8147